Changes in large-scale climate alter spatial synchrony of aphid pests

Lawrence W. Sheppard[1]*, James R. Bell[2], Richard Harrington[2] and Daniel C. Reuman[1,3]*

Spatial synchrony, the tendency of distant populations to fluctuate similarly, is a major concern in ecology[1-8]. Except in special circumstances[3,9], researchers historically had difficulty identifying drivers of synchrony in field systems[5,6,10]. Perhaps for this reason, the possibility[9,11,12] that changes in large-scale climatic drivers may modify synchrony, thereby impacting ecosystems and human concerns, has been little examined. Here, we use wavelets to determine environmental drivers of phenological synchrony across Britain for 20 aphid species, most major crop pests. Consistently across species, changes in drivers produced large changes in aphid synchrony. Different drivers acted on different timescales: using a new wavelet analogue of the Moran theorem[1], we show that on long timescales (>4 years), 80% of synchrony in aphid first flights is due to synchrony in winter climate; but this explanation accounts for less short-timescale (≤4 years) synchrony. Changes in aphid synchrony over time also differed by timescale: long-timescale synchrony fell from before 1993 to after, caused by similar changes in winter climate; whereas short-timescale synchrony increased. Shifts in winter climate are attributable to the North Atlantic Oscillation, an important climatic phenomenon[7,11,13], so effects described here may influence other taxa. This study documents a new way that climatic changes influence populations, through altered Moran effects.

Spatial synchrony is defined as the tendency of spatially separated populations of a species to fluctuate in a similar way. Synchrony can affect regional ecosystem functioning[14-17]: asynchronous local population fluctuations negate each other in the regional average population and hence have limited influence; but synchronization can result in large-scale outbreaks, shortages[18-20] or extinctions[21].

Annual time series from 1976 to 2010 for 20 aphid species' first flight day, flight duration (length of the flying season), and total annual count were extracted from the Rothamsted Insect Survey suction-trap data set (Methods) for 11 locations spanning Britain (Supplementary Table 1). The survey includes daily counts of hundreds of species from many locations. Locations were selected for their duration of operation. Species (Supplementary Table 2) were selected before analyses for their importance as pests and model species for population dynamics studies[22,23]. Data for potential environmental drivers for the sites for the same years were used. Analyses examining average winter (December–March), April, and May temperatures are presented here. British aphids are a classic system for studies of synchrony[2,24], but changes in synchrony have not been examined.

The strength of population synchrony can differ by timescale[20] and can change over time[25]. These features can be detected with the wavelet mean field (Methods and Supplementary Fig. 1), a technique that provides a plot showing strength of synchrony as a function of timescale and time. The wavelet mean field is an average of normalized wavelet transforms of available time series.

Using wavelet mean fields we found marked timescale structure and substantial changes in aphid first-flight synchrony. Patterns were consistent across all but two species. We compared two 17-year-long parts of each species' wavelet mean field, dividing the study period into equally sized early and late halves. To summarize timescale structure we compared the part of the mean field describing long timescales (period > 4 years, corresponding to Fourier components with positive lag-1 autocorrelation) with the part describing short timescales (period ≤ 4 years, Fourier components with negative lag-1 autocorrelation). First-flight synchrony was biased towards longer timescales for the first 17 years of the study period, 1976–1992 (Fig. 1a arrow tails, $p = 1.1 \times 10^{-6}$, p values in this paragraph are from paired t-tests across species). For the period after 1993, long-timescale synchrony dropped significantly ($p = 7.4 \times 10^{-9}$, Fig. 1a cyan arrows) by an average of 35%, and short-timescale synchrony increased ($p = 1.2 \times 10^{-3}$, Fig. 1a green arrows) by 26%, with the result that short-timescale synchrony dominated in 1994–2010 ($p = 2.4 \times 10^{-6}$, Fig. 1a arrow heads). The only two species for which long-timescale synchrony did not decrease markedly were the corn leaf aphid (*Rhopalosiphum maidis*; species 6) and the sycamore aphid (*Drepanosiphum platanoidis*; species 19).

Observed changes in synchrony may have important implications for pest management: the balance of long- and short-timescale synchrony determines year-to-year volatility of average first flight times, and observed changes mean volatility increased. Before 1993, when first flight times were synchronized predominantly on long timescales, time series of species-average first flight times across Britain were dominated by low frequencies because synchronized long-timescale fluctuations reinforced each other in the average but short-timescale fluctuations tended more to cancel out. Thus, average timing of flights changed slowly from year to year. When long-timescale synchrony was replaced by short-timescale synchrony after 1993, high-frequency oscillations in local first flight times occurred more in unison across Britain, so timing of average first flights became dominated by high frequencies, and was more volatile. These changes can be detected using lag-1 autocorrelations (Supplementary Fig. 2), which decreased significantly ($p = 7.2 \times 10^{-8}$, paired t-test) from an average of 0.234 before 1993 to −0.203 after; although it would have been difficult to know to look for this change without first having done a systematic wavelet or equivalent analysis. This constitutes a change from persistent to anti-persistent dynamics with respect to year-to-year changes in UK-average phenology.

Flight durations and total counts were also synchronized, and species often showed changes in synchrony and its timescale

[1]Department of Ecology and Evolutionary Biology and Kansas Biological Survey, University of Kansas, Lawrence, Kansas 66047, USA. [2]Rothamsted Insect Survey, Rothamsted Research, West Common, Harpenden AL5 2JQ, UK. [3]Laboratory of Populations, Rockefeller University, 1230 York Avenue, New York 10065, USA. *e-mail: lwsheppard@ku.edu; reuman@ku.edu
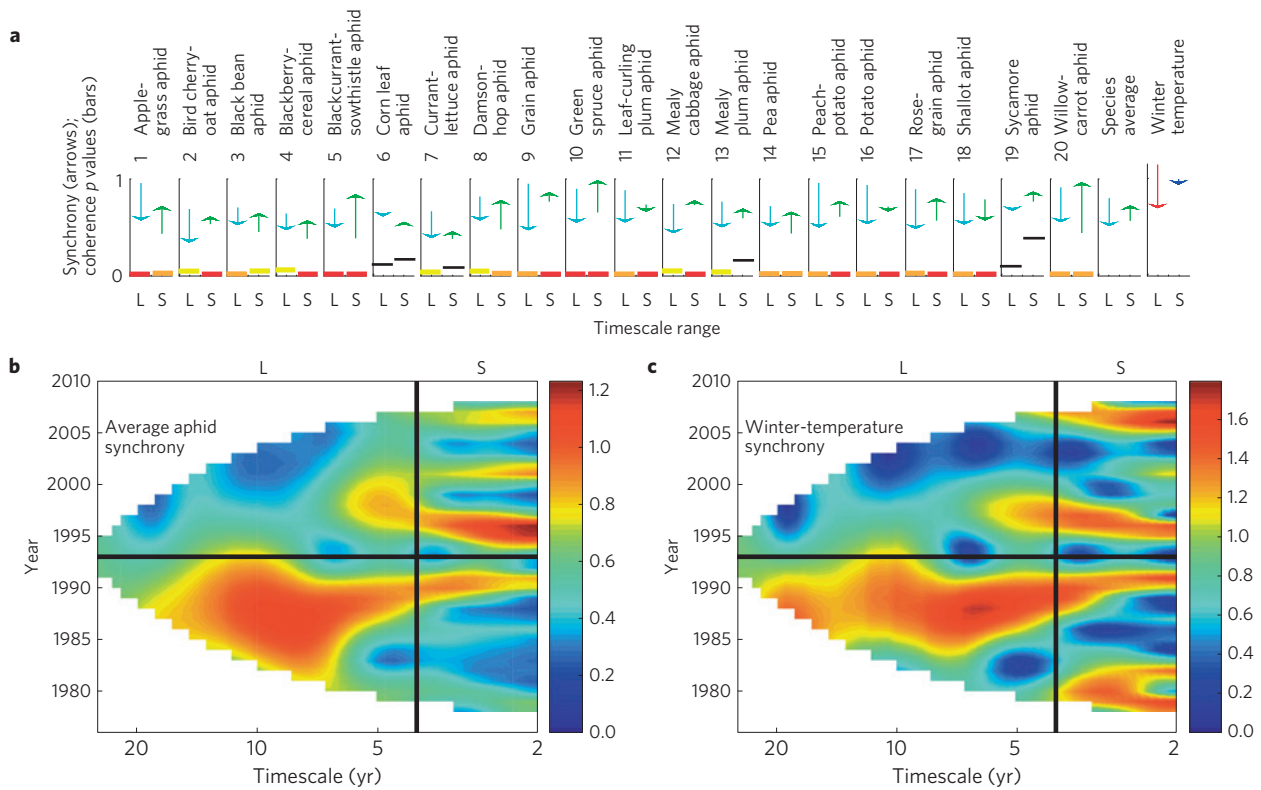
Figure 1 | Synchrony of aphid first flights changed, driven by synchrony in winter climate. a, Arrows go from values representing strength of synchrony in 1976–1992 to values for 1994–2010 for long (L, cyan; >4 years) and short (S, green; 4 years) timescales; tips and tails are averages of wavelet mean field magnitudes (Methods). Bar heights and colours show *p* values for spatial coherences between first flights and winter temperatures. Red *p* < 0.001; orange *p* < 0.01; yellow *p* < 0.05. **b,c**, Surface plots show wavelet mean field magnitudes representing synchrony (red) and asynchrony (blue), averaged across aphid species (**b**), and for winter temperatures (**c**).

structure, but regularities across species were not observed (Supplementary Figs 3 and 4). Total count and flight duration are subject to many factors acting on the reproduction of the aphids through the year. These variables may be considered composite variables, in the sense that they are functions of several simpler variables. For instance, flight duration is influenced by first flights and last flights, which are themselves subject to different regulating factors. The variability of total count and flight duration thus may be less subject to single controlling factors than first flight.

Winter-temperature synchrony on long timescales also decreased from before to after 1993 (Fig. 1a, red arrow), and in fact detailed patterns of how synchrony depends on time and timescale were strikingly similar for winter temperatures and on average across species for first flights (Fig. 1b,c). This similarity suggests, but does not prove, the hypothesis that winter-temperature synchrony causes first-flight synchrony. To formally test this hypothesis, we evaluated wavelet spatial coherences for long and short timescales for each species. Spatial coherence measures the extent to which two variables have consistent phase differences and correlated magnitudes of oscillation over time at all locations of measurement, as a function of timescale (Supplementary Fig. 5 and Methods). As oscillations in aphid variables cannot plausibly cause oscillations in environmental variables, a significant spatial coherence shows a causal effect of the environmental variable, or one highly coherent with it, on the aphid variable[26]. This is because irregular oscillators that are not causally related are unlikely to maintain consistent phase differences or magnitude correlations over time.

Winter temperatures were strongly spatially coherent with first flights (Fig. 1a, horizontal bars), supporting the hypothesis that these variables are causally related. Additional evidence also

supports the hypothesis. First, the only two species not showing significant spatial coherence with winter temperatures were the corn leaf and sycamore aphids, the same two species that did not show changes in synchrony consistent with winter temperature. Second, species overwintering in active life stages (codes 6, 9, 10, 15, 16, 18, Fig. 1) were significantly more spatially coherent with winter temperature than species overwintering as eggs (1, 3, 4, 5, 7, 8, 13, 17, 19), which are less susceptible to cold (average factor 1.23, $p = 7.5 \times 10^{-3}$ for long; average factor 1.41, $p = 0.030$ for short timescales, one-tailed *t*-tests). April and May temperatures were not generally spatially coherent with first flight (Supplementary Fig. 6), even though April and May are closer to when aphids first fly (April–July) than is winter.

Some relationships with winter temperature in Fig. 1 can be explained by known mechanisms. Active overwinterers are adversely affected by low temperatures and outbreak after mild winters[22,27]. Overwintering eggs of aphids are very tolerant of low temperature whereas mobile stages are not. Mobile stages suffer direct mortality if temperatures fall sufficiently low for a sufficient length of time, threshold values varying with species and clone. At higher low-temperature thresholds and shorter durations, sublethal effects on the development and fecundity of offspring can occur. Movement by walking is also inhibited. For all of these reasons, the abundance of aphids in spring, and hence the time of first detection in traps, is expected to be more closely linked to winter temperature in species overwintering in mobile stages rather than as eggs. Mechanisms may also be indirect: cereal aphid outbreaks are related to the previous winter for some species owing to wheat phenology[22]. Flight duration and count fluctuations were also sometimes spatially coherent with winter temperatures, but less consistently than first flight (Supplementary Fig. 6).
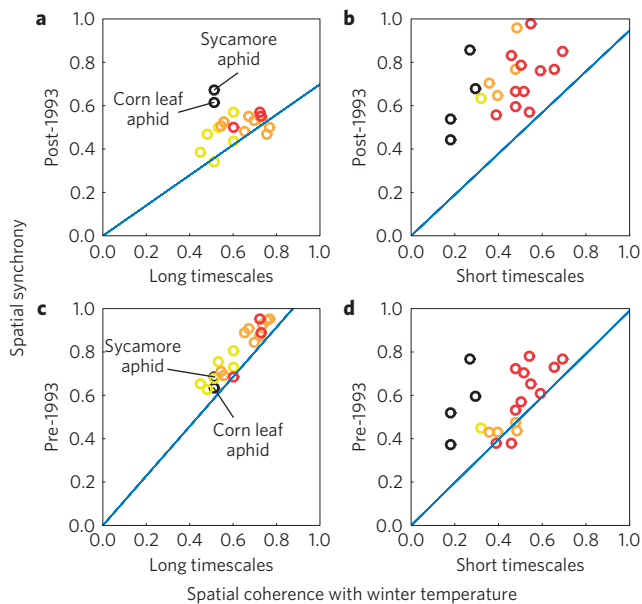
Figure 2 | Inter-species variation and changes in synchrony are explained by winter climate. a–d, Species marker heights represent strengths of first-flight synchrony. Horizontal displacements are spatial coherences of first flights with winter temperatures, colours representing significance as in Fig. 1a. Lines are expected synchrony, according to the wavelet Moran theorem, if winter temperature were the sole synchronizing influence. Vertical distances between points and lines represent residual synchrony from other influences. Line slopes are strengths of winter-temperature synchrony. **a,c**, On long timescales, residual synchrony is minimal, species with greater coherence are more synchronized, and reductions from before 1993 to after generally follow reductions in winter-temperature synchrony. Mathematical details are given in 'Moran theorem' results in Methods.

To explore further the influence of winter-climate synchrony on first-flight synchrony, we developed a timescale-specific version of the Moran theorem, a classic theorem relating population synchrony to synchrony of environmental fluctuations[1]. In words, the new theorem states that at timescale σ, if the only synchronizing influence on a biological variable, b, is the environmental variable e, then the strength of biological synchrony is the strength of synchrony in the environmental driver times the coherence of that driver with the biological variable. Precisely, $\langle |r_\sigma^{(b)}(t)| \rangle \approx \langle |r_\sigma^{(e)}(t)| \rangle |\Pi_\sigma^{(be)}|$, where the r_σ are wavelet mean fields (superscripts (b) and (e) indicating the two variables), $|\cdot|$ represents complex magnitude, $\langle\cdot\rangle$ is the square root of the time-averaged squared value (r.m.s.), and $|\Pi_\sigma^{(be)}|$ is spatial coherence. The left side measures biological synchrony and the first multiplicand measures environmental synchrony. The theorem formalizes the reasoning that synchrony of a driven variable should depend on synchrony of the driver and the strength of its influence. Additional independent influences may exist that increase biological synchrony, turning the approximate equality, $\approx$, into an inequality, $>$. The right side of the formula is then the amount of synchrony attributable to the environmental variable e, with the remaining synchrony attributable to the action of these other factors.

If winter-climate synchrony is indeed the principal driver of first-flight synchrony, the theorem provides three expectations: the right side of the equation will be close in magnitude to the left side for winter temperatures and first flights; species with greater spatial coherence with winter temperatures will be more synchronized; and changes over time in winter-temperature synchrony will be parallelled by proportional changes in first-flight synchrony. On long timescales, all three expectations were met for the 18 species excluding the corn leaf and sycamore aphids (Fig. 2a,c). First, winter-temperature synchrony explained an average of 80% of
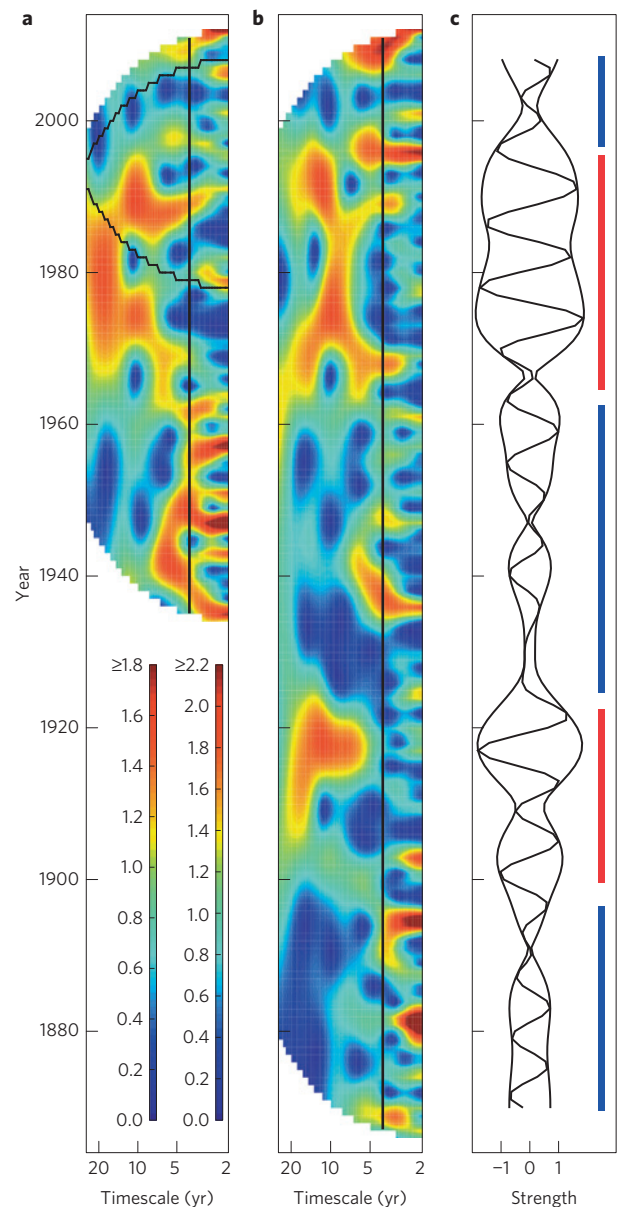

Figure 3 | Changes in winter-temperature synchrony mirrored changes in the NAO. a, Wavelet mean field magnitudes for winter temperatures from 13 long-maintained UK weather stations resembled their counterparts for the 11 aphid sampling locations (Fig. 1c); the comparable part of the plot is indicated by black lines. **b**, A normalized wavelet transform of Hurrell's winter NAO index showed similar features to **a** on long timescales (4–27 years). The real part of the 10-year-timescale component of this NAO transform is plotted in **c. c**, The envelope enclosing the fluctuations is the height of **b** at 10-year timescale. Times for which long-timescale NAO oscillations were strong (red) or weak (blue) are also marked in **c**.

long-timescale synchrony (see Methods for how this value is calculated). Second, species more coherent with winter temperature were more synchronized. Third, and most importantly, the decrease in winter-temperature synchrony from before to after 1993 was parallelled by a decrease in first-flight synchrony. In contrast, short-timescale first-flight synchrony was much greater than expected if winter temperatures were the only synchronizing influence on those timescales (Fig. 2b,d), indicating that additional influences exist. Although winter-temperature synchrony changed minimally on short timescales, first-flight synchrony increased owing to the other influences.

The observed long-timescale changes in winter-temperature synchrony, shown to have caused changes in first-flight synchrony, were in turn related to changes in the North Atlantic Oscillation (NAO). On long timescales, wavelet mean fields of winter temperatures for our 11 sampling locations, and also for 13 long-running weather stations across the UK (see Methods and Supplementary Table 3), resembled wavelet transforms of Hurrell's NAO index (Fig. 3a,b and Methods). Coherences between the NAO index and winter temperatures were significant on long timescales (aphid sampling locations, $p = 0.017$; long-running stations, $p = 2.6 \times 10^{-3}$). Thus, on long timescales, the synchronous component of winter temperatures in the UK is largely controlled by the NAO. The change around 1993 in long-timescale winter-temperature synchrony (Fig. 1c) also manifests as a change in the NAO (Fig. 3b). Similar changes in the NAO occurred previously with multidecadal spacing (Fig. 3b,c). Although it is unsurprising that the NAO affects winter-temperature synchrony because the NAO has known importance for winter climate, relating changes in aphid synchrony to the NAO, as our results do, is important because the NAO has widespread ecological influence[11,13,25] and hence changes in synchrony as we observed may be seen broadly in other locations and taxa[25].

Our results could probably not be obtained if we were unable to disaggregate synchrony by timescale. For instance, population synchrony has previously been measured by computing correlations between population time series at all pairs of locations and averaging; and strength of relationship between population and environmental variables has previously been measured by computing correlations between them in all locations and averaging. First-flight synchrony and strength of relationship between first flight and winter temperature were uncorrelated across species when measured in these ways (Pearson test, $p = 0.74$), contrasting with the results of Fig. 2a,c. As different mechanisms can drive synchrony on different timescales, combining timescales using correlation approaches[17,28] obscures causal influences[10,19,20,29] that our methods can reveal.

This study demonstrates a new way in which environmental changes can affect populations on large spatial scales. Changes in the relationships between local environmental drivers, more so than changes in those drivers themselves, altered regional aphid dynamics; thus, mechanisms were fundamentally different from widely studied effects of climate on phenology and species ranges. Moran effects, of which the observed phenomena are an aspect, are thought to be widespread[4,6,7,30], especially for winter-climatic drivers in temperate regions[3,9,13,16,25]. The NAO affects climate and many species across a wide area[11,13,25]. It is therefore reasonable to expect that the phenomena explored here may be seen broadly.

Methods

Methods and any associated references are available in the online version of the paper.

References

1. Moran, P. The statistical analysis of the Canadian lynx cycle, II. *Aust. J. Zool.* **1,** 291–298 (1953).
2. Hanski, I. & Woiwod, I. Spatial synchrony in the dynamics of moth and aphid populations. *J. Anim. Ecol.* **62,** 656–668 (1993).
3. Grenfell, B. *et al.* Noise and determinism in synchronized sheep dynamics. *Nature* **394,** 674–677 (1998).
4. Lande, R., Engen, S. & Sæther, B. Spatial scale of population synchrony: Environmental correlation versus dispersal and density regulation. *Am. Nat.* **154,** 271–281 (1999).
5. Bjørnstad, O., Ims, R. & Lambin, X. Spatial population dynamics: Analyzing patterns and processes of population synchrony. *Trends Ecol. Evol.* **14,** 427–432 (1999).
6. Liebhold, A., Koenig, W. & Bjørnstad, O. Spatial synchrony in population dynamics. *Annu. Rev. Ecol. Evol. Syst.* **35,** 467–490 (2004).
7. Engen, S., Lande, R., Sæther, B. & Bregnballe, T. Estimating the pattern of synchrony in fluctuating populations. *J. Anim. Ecol.* **74,** 601–611 (2005).
8. Vasseur, D. & Fox, J. Phase-locking and environmental fluctuations generate synchrony in a predator–prey community. *Nature* **460,** 1007–1010 (2009).
9. Post, E. & Forchhammmer, M. Synchronization of animal population dynamics by large-scale climate. *Nature* **420,** 168–171 (2002).
10. Abbott, K. Does the pattern of population synchrony through space reveal if the Moran effect is acting? *Oikos* **116,** 903–912 (2007).
11. Stenseth, N. *et al.* Ecological effects of climate fluctuations. *Science* **297,** 1292–1296 (2002).
12. Ojanen, S., Niemenen, M., Meyke, E., Pöyry, J. & Hanski, I. Long-term metapopulation study of the Glanville fritillary butterfly (*Melitaea cinxia*): Survey methods, data management, and long-term population trends. *Ecol. Evol.* **3,** 3713–3737 (2013).
13. Ottersen, G. *et al.* Ecological effects of the North Atlantic Oscillation. *Oecologia* **128,** 1–14 (2001).
14. Bjørnstad, O., Peltonen, M., Liebhold, A. & Baltensweiler, W. Waves of larch budmoth outbreaks in the European alps. *Science* **298,** 1020–1023 (2002).
15. Beaugrand, G., Brander, K., Lindley, J., Souissi, & Reid, P. Plankton effect on cod recruitment in the North Sea. *Nature* **426,** 661–664 (2003).
16. Stenseth, N. *et al.* The effect of climatic forcing on population synchrony and genetic structuring of the Canadian lynx. *Proc. Natl Acad. Sci. USA* **101,** 6056–6061 (2004).
17. Haynes, K., Bjørnstad, O., Allstadt, A. & Liebhold, A. Geographic variation in the spatial synchrony of a forest-defoliating insect: Isolation of environmental and spatial drivers. *Proc. R. Soc. B* **280,** 20122373 (2013).
18. Micheli, F. The dual nature of community variability. *Oikos* **85,** 161–169 (1999).
19. Vasseur, D. & Gaedke, U. Spectral analysis unmasks synchronous and compensatory dynamics in plankton communities. *Ecology* **88,** 2058–2071 (2007).
20. Keitt, T. Coherent ecological dynamics induced by large-scale disturbance. *Nature* **454,** 331–335 (2008).
21. Earn, D., Levin, S. & Rohani, P. Coherence and conservation. *Science* **290,** 1360–1364 (2000).
22. Dixon, A. *Aphid Ecology: An Optimization Approach* 2nd edn (Chapman and Hall, 1998).
23. Van Emden, H. & Harrington, R. *Aphids as Crop Pests* (CAB International, 2007).
24. Estay, S., Lima, M. & Harrington, R. Climate mediated exogenous forcing and synchrony in populations of the oak aphid in the UK. *Oikos* **118,** 175–182 (2009).
25. Post, E. & Forchhammer, M. C. Spatial synchrony of local populations has increased in association with the recent northern hemisphere climate trend. *Proc. Natl Acad. Sci. USA* **101,** 9286–9290 (2004).
26. Sheppard, L. W., Stefanovska, A. & McClintock, P. V. E. Testing for time-localized coherence in bivariate data. *Phys. Rev. E* **85,** 046205 (2012).
27. Harrington, R., Bale, J. & Tatchell, G. in *Insects in a Changing Environment* (eds Harrington, R. & Stork, N.) 125–155 (Academic, 1995).
28. Bjørnstad, O. & Falck, W. Nonparametric spatial covariance functions: Estimation and testing. *Environ. Ecol. Stat.* **8,** 53–70 (2001).
29. Fontaine, C. & Gonzalez, A. Population synchrony induced by resource fluctuations and dispersal in an aquatic microcosm. *Ecology* **86,** 1463–1471 (2005).
30. Peltonen, M., Liebhold, A., Bjørnstad, O. & Williams, D. Spatial synchrony in forest insect outbreaks: Roles of regional stochasticity and dispersal. *Ecology* **83,** 3120–3129 (2002).

Author contributions

L.W.S. and D.C.R. designed and carried out the analysis and wrote the paper. Data and interpretive assistance were provided by J.R.B. and R.H. All authors contributed to editing.

Additional information

Supplementary information is available in the online version of the paper. Reprints and permissions information is available online at www.nature.com/reprints. Correspondence and requests for materials should be addressed to L.W.S. or D.C.R.

Competing financial interests

The authors declare no competing financial interests.

Methods

Data. Aphid counts, usually daily, were available from the Rothamsted Insect Survey[31,32] for all 20 species and 11 sites throughout the flight season. Aphid recording sites and their active periods are in Supplementary Table 1. Some daily counts were estimates based on subsampling, when aphid catches were particularly high. The Julian date at which the first aphid of a given species was recorded at a site in a given year was taken as the first flight day for that species, site and year. When samples included more than one day's catch, the first day in the first period to have a non-zero catch was used. The total count over all days of the year for which aphids of a given species were recorded was taken as the count for that year. To determine flight duration, 5 and 95% quantiles of the total year's count were determined, and the Julian dates at which those thresholds were exceeded were computed. The difference was flight duration. If the count for a given species, year and site was zero, the flight duration was taken to be zero and the first flight date was taken to be the latest first flight date observed in other years for that species and site. For the 3.38% of site-years for which no data were available for a year the median values found at that site over other years were used for first flight, flight duration and count. This fraction of data that were missing is small, and data were missing in patterns unrelated across sampling locations, so replacing missing data with medians will have added noise and reduced significances of detected patterns, but could not artefactually have produced the results we report. Lists of active and egg overwinterers excluded species that commonly show both behaviours in the UK.

Aphid suction-trap locations were deliberately chosen (decades ago) to give as much coverage of the UK as possible, commensurate with staffing resources. However, notable gaps in the suction trapping network are Wales, Northern Ireland, and central southern England. It is possible, a priori, that patterns or causes of synchrony in these areas differ from the patterns described in our results.

Monthly temperature time series were averaged across winter months. Winter was always taken to be December–March. Two of Hurrell's winter NAO time series indices were used, one based on the difference of normalized sea level pressure between weather stations in Lisbon and Reykjavik[33], and the other based on principal component time series from empirical orthogonal function analysis of sea level pressure fields in a whole region of the North Atlantic[34]. Results in Fig. 3 use the former, but results using the latter were substantially the same. In addition to the winter-temperature measurements at the aphid sampling locations, 13 long-duration time series of winter temperature[35] were used for comparison to the NAO indices. These spanned 1932–2014 and were from the locations in Supplementary Table 3.

Wavelet mean field. If $x(t)$ $(t = 1, \ldots, T)$ is a time series, then the wavelet transform at timescale (period) σ and time t, $W_\sigma(t)$, is a complex number with magnitude and phase that can be interpreted as the strength and phase of oscillation in $x(t)$ at timescale σ and time t. The specific transform used is defined precisely below. Wavelet methods have been used often in ecology[20,36–42] and general introductions[43,44] are readily available.

If $x_n(t)$ $(t = 1, \ldots, T)$ is the nth of N time series from different locations, and $W_{n,\sigma}(t)$ is its wavelet transform, then the wavelet mean field is

$$r_\sigma(t) = (1/N) \sum_{n=1}^{N} w_{n,\sigma}(t), \quad \text{where}$$

$$w_{n,\sigma}(t) = W_{n,\sigma}(t) \Big/ \sqrt{(1/NT) \sum_{n=1}^{N} \sum_{t=1}^{T} W_{n,\sigma}(t) \overline{W_{n,\sigma}(t)}}$$

Overbar denotes complex conjugation. The $w_{n,\sigma}(t)$ are power-normalized transforms in the sense that the denominator in the previous expression is the square root of the average wavelet power of the time series over sampling locations. As that denominator is only a single positive rescaling factor, the $w_{n,\sigma}(t)$ contain essentially the same information as the $W_{n,\sigma}(t)$. In particular, the phases of $w_{n,\sigma}(t)$ and $W_{n,\sigma}(t)$ are the same, equal to the phase of oscillation in $x_n(t)$ at time t and timescale σ.

The magnitude of the wavelet mean field makes sense as a time- and timescale-specific measure of the strength of synchrony because when oscillations at time t and timescale σ have similar phase in all time series, and are therefore synchronized, the sum $\sum_{n=1}^{N} w_{n,\sigma}(t)$ will be a large complex number, whereas unrelated phases will tend to produce a small sum. The wavelet mean field is also a natural choice because of its mathematical properties. The mean squared magnitude of the wavelet mean field, $(1/T) \sum_{t=1}^{T} |r_\sigma(t)|^2$, is between 0 and 1, and equals 1 for all σ if and only if the time series $x_n(t)$ $(t = 1, \ldots, T)$ are identical (Supplementary equations, lemma 1). Also, this quantity is the power of the average time series divided by the average of the powers of all the time series (Supplementary equations, lemma 1). If time series are unsynchronized, power in the average time series will tend to be reduced, as unsynchronized fluctuations will cancel. In contrast, synchronized fluctuations will reinforce each other and contribute power to the average. In this way $(1/T) \sum_{t=1}^{T} |r_\sigma(t)|^2$ represents synchrony for each timescale, σ. It is the

wavelet generalization of var $((1/N) \sum_{n=1}^{N} x_n(t))/((1/N) \sum_{n=1}^{N} \text{var}(x_n(t)))$ (Supplementary equations, lemma 1), a familiar quantity readily interpretable as synchrony because it represents the extent to which oscillations in local time series reinforce each other or cancel in the average time series. Methods related to the wavelet mean field have been used previously to study synchrony in ecology[20,36–38].

Arrow tips and tails in Fig. 1a were obtained by averaging $|r_\sigma(t)|^2$ over the time period before or after 1993 and then averaging the square root of the result over long or short timescales. Figure 1b was obtained by producing a wavelet mean field magnitude plot for each species, and then averaging across species for each time and timescale. The dividing year, 1993, between the two periods considered and the dividing timescale, 4 years, between long and short timescales were chosen after inspecting wavelet mean field magnitude plots for these reasons: 1993 divides the data into two equal (and therefore easily comparable) parts; and 1 cycle every 4 years was exactly half the Nyquist frequency for annual sampling and is a boundary between persistent and anti-persistent behaviour in sinusoidal oscillations (Fourier components), as measured by the lag-1 autocorrelation. Wavelet transform magnitudes of NAO indices were divided by the power at each timescale in Fig. 3b, for comparability with wavelet mean field plots, which used a similar power normalization (above).

We used a continuous complex Morlet wavelet transform[44]. The mother wavelet was $\Psi(t) = (e^{i2\pi f_0 t} - e^{-(2\pi f_0)^2/2}) \exp(-t^2/2)$, with $f_0 = 0.5$. Wavelets associated with a range of timescales were produced using rescaling: $\Psi_\sigma(t) = s^{-1/2}(e^{i2\pi f_0 t/s} - e^{-(2\pi f_0)^2/2}) \exp(-t^2/2s^2)$. Following convention[41] we identify each wavelet with a characteristic timescale, $\sigma = s/f_0$, and characteristic frequency, $f = f_0/s$. The actual peak in the Morlet wavelet power spectrum of a sinusoid signal with frequency f', period $\sigma' = 1/f'$, is at $s = ((2\pi f_0 + (2 + (2\pi f_0)^2)^{1/2})/4\pi)(\sigma')$, so $f \approx f'$ (ref. 45). The centre frequency f_0 of the mother wavelet, which has width $s = 1$ and $\sigma = 2$, was taken to be 0.5 to give a high degree of temporal resolution, but necessitating the subtraction of a constant to keep the mean of the wavelet equal to zero[44]. The mother wavelet was scaled so that one wavelet oscillation was equal to two years, that is, $\sigma = 2$, because a two-year period corresponds to the highest-frequency fluctuation that can be identified in an annual time series. Wavelets with a range of periods from 2 years to over 27 years were generated, starting with $\sigma = 2$ and multiplying each period by 1.05 to get the next. Convolving a time series $x_n(t)$ from location n with wavelets having different periods produces a set of complex wavelet components $W_{n,\sigma}(t) = \sum_{t'} x_n(t + t')\Psi_\sigma(t')$. The transform is scalloped to remove poorly estimated values[44], specifically where the wavelet envelope at the edge of the time series in the convolution has 1% or more of its maximum amplitude.

Spatial coherence. The spatial coherence of biological (b) and environmental (e) variables $x_n^{(b)}(t)$ and $x_n^{(e)}(t)$ is the magnitude of the quantity $\Pi_\sigma^{(be)} = (1/NT) \sum_{n=1}^{N} \sum_{t=1}^{T} w_{n,\sigma}^{(b)}(t) \overline{w_{n,\sigma}^{(e)}(t)}$, and takes values between 0 and 1 (Supplementary equations, lemma 2). As $w_{n,\sigma}^{(b)}(t) \overline{w_{n,\sigma}^{(e)}(t)}$ is a complex number with a phase equal to the phase difference between the two wavelet components, the total (summed over n and t) is large if the phase difference is consistent over time and across locations, and small otherwise. The wavelet components can also have varying magnitudes, and the spatial coherence is further increased if there are correlations in the amplitudes of the fluctuations. Thus, the spatial coherence measures the extent to which the two variables have consistent phase differences and correlated magnitudes over time and across locations, as a function of timescale. The spatial coherence indicates the strength of relationship between the variables whether they are in phase or phase shifted. For a single site ($N = 1$), the spatial coherence is the (standard) wavelet coherence[43,44] of the two variables at that site. The measure also relates to the phase coherence[36,37,46,47]. Coherences between winter-temperature variables and NAO indices were computed with the spatial coherence formula (above) but with $x_n^{(b)}(t)$ taken to be winter temperature and $x_n^{(e)}(t)$ taken to be the NAO index time series for all n.

We developed our methods in application to spatially referenced time series and refer to them using terminology that references spatial applications (for example, we use the term 'spatial coherence'). However, our methods are applicable to simultaneous time series with or without spatial separation and referencing, a slightly more general context. For example, the methods could be used to study inter-species synchrony of plankton density fluctuations in a single pond.

Surrogate data sets for statistical significance. The level of spatial coherence consistent with the null hypothesis that there is no relationship between two variables depends on both the temporal and spatial autocorrelation of the data. For instance, two variables that oscillate regularly at the same frequency and are both highly spatially synchronized will have a phase difference that is very consistent over time and space, and therefore high spatial coherence, even if they are not related; two irregular oscillators with low spatial synchronization are much less likely to exhibit consistent phase differences over time and space if unrelated. We tested spatial coherences for significance through a resampling method based on Fourier surrogate data sets. Our method is a straightforward extension of the

widely used Fourier surrogate method[48,49]. Surrogates randomize away phase relationships between variables while retaining the same spatial and temporal autocorrelation properties of each variable (see below for details on how to produce surrogates). Thus, evaluating the spatial coherences of large numbers of these surrogate data sets makes it possible to produce a distribution of spatial coherence values consistent with the null hypothesis of no relationship, for comparison with the spatial coherence of the data. For all tests, 10,000 surrogates were used. To produce significance values separately for long (>4 years) and short (≤4 years) timescales, the rank of the spatial coherence relative to surrogates was found at each timescale (rank 1 was highest), and then the mean rank was computed inside the long- and short-timescale ranges. The same procedure applied to each one of the surrogates produced surrogate mean ranks in the two ranges of timescales, and the proportion of surrogate mean ranks less than the actual mean rank provided the p values presented, for example, in Fig. 1a (horizontal bars). Other methods exist for determining environmental causes of synchrony[4,7,17,50–52]; we used wavelet tools because they naturally cope with heterogeneity across times and timescales in the phenomena examined.

Given time series $x_n(t)$ in locations $n = 1, \ldots, N$, we generated surrogate time series for all N locations simultaneously, which we here call whole-Britain surrogates. We Fourier transformed the N time series, phase randomized the Fourier components by the addition of a random phase at each frequency, and inverse transformed. The resulting time series have the same power spectrum as the original time series, and hence the same autocorrelation properties, but have different temporal structure. For each frequency, f, the same random phase was added to Fourier components corresponding to f for each of the N time series. Thus, our Fourier surrogates also preserve the cross spectrum and cross-correlation properties of the N time series. We produced these whole-Britain surrogates independently for aphid and environmental time series, so that between aphid and environmental variables the cross spectra, correlations and spatial coherences were not preserved, and thus the surrogates represent the null hypothesis of no relationship. Surrogate approaches to obtaining significance for wavelet analyses are standard[41,42,48,49,53].

Box–Cox transformations. Fourier surrogates described in the previous section tend to have normal marginal distributions[53], so significance testing based on those surrogates can be applied only to data that also have normal marginals. Raw time series sometimes had non-normal marginals. Therefore, we normalized data before analysis using a straightforward multi-time-series version of standard optimal Box–Cox transformation techniques[54]. Transformations used a different Box–Cox coefficient for each variable, but the same coefficient for all sites for a variable, determined as follows. The time series for each of the 11 sites was adjusted to have a minimum value of one by the addition of a constant. Then Box–Cox transformations with a range of coefficients were applied, and for each coefficient the maximum likelihood variance, mean and slope parameters were found for a model of the transformed variable with a Gaussian distribution about a linear trend. The log likelihood was recorded. For each coefficient, the sum of the log likelihoods at all sites was found, and the coefficient giving the greatest total log likelihood was selected and used for all the time series. A linear trend was then subtracted and the standard deviation rescaled to one for each time series, giving zero-mean time series with no trend and unit variance. The procedure was applied separately to each of the three types of time series (first flight, flight duration, count) for each of the 20 species, and to the environmental variables. Optimal Box–Cox transformations turned out to be approximately linear for first flight, and similar to log transformations for count.

Moran theorem results. A proof of the wavelet Moran theorem is in Supplementary equations, theorem 3. Species marker heights on Fig. 2 are timescale-averaged (over long or short timescale) root mean square (r.m.s.; mean over the period before or after 1993) wavelet mean field magnitudes for aphid first flights (compute $|r_\sigma^{(b)}(t)|^2$, average over the appropriate time window, take the square root, and then average over the appropriate frequency band). Horizontal marker displacements are timescale-averaged spatial coherences of first flights with winter temperature, with coherences determined over 1976–2010. Diagonal lines have slopes equal to the timescale-averaged r.m.s. wavelet mean field of winter temperatures, with averages again over the timescale band and time period of interest. Vertical distances between points and lines correspond to residual synchrony, from influences other than winter temperature.

Species marker heights on Fig. 2 will tend to be in the interval $[0, 1]$ even though wavelet mean field magnitude values at particular times and timescales need not be in that interval (see Fig. 1b), because lemma 1 in Supplementary equations proves that the time-averaged quantity $(1/T)\sum_{t=1}^{T}|r_\sigma(t)|^2$ must be in the interval $[0, 1]$. For a given timescale, the quantity $|r_\sigma(t)|^2$ can exceed 1 for a given t if it is less than 1 for other t. The same reasoning applies to the arrow tail and head heights in Fig. 1a, as these quantities are the same as the species marker heights in Fig. 2. Even time averages of $|r_\sigma(t)|^2$ over a subset of the times $1, \ldots, T$

(for instance over the years before or after 1993) can exceed 1, as in the right-most panel in Fig. 1a, but this is less common owing to the greater averaging.

The Moran theorem equation in the main text is a timescale-by-timescale statement, but Fig. 2 uses averages across long or short timescales for all quantities, an approximation made for conceptual clarity. An exact version of the figure (Supplementary Fig. 7) illustrates that this approximation makes essentially no difference. The details of what is plotted in Supplementary Fig. 7 are explained in Supplementary Notes.

The fraction of synchrony explained for a species for a timescale band was obtained by averaging the quantity $|\Pi_\sigma^{(be)}|^2 \left\langle |r_\sigma^{(e)}(t)| \right\rangle^2 / \left\langle |r_\sigma^{(b)}(t)| \right\rangle^2$ over the band.

Code availability. Matlab codes for the wavelet mean field, complex Morlet wavelet transform, spatial coherence, and surrogates are available from the authors on request.

References

31. Macaulay, E., Tatchell, G. & Taylor, L. The Rothamsted Insect Survey 12-metre suction trap. *Bull. Entomol. Res.* **78,** 121–129 (1988).
32. Harrington, R. The Rothamsted Insect Survey strikes gold. *Antenna* **38,** 158–166 (2014).
33. Hurrell, J. & National Center for Atmospheric Research Staff. *The Climate Data Guide: Hurrell North Atlantic Oscillation (NAO) Index (Station-based)* (NCAR, accessed 15 January 2015); https://climatedataguide.ucar.edu/climate-data/hurrell-north-atlantic-oscillation-nao-index-station-based
34. National Center for Atmospheric Research Staff. *The Climate Data Guide: Hurrell North Atlantic Oscillation (NAO) Index (PC-based)* (NCAR, accessed 15 January 2015); https://climatedataguide.ucar.edu/climate-data/hurrell-north-atlantic-oscillation-nao-index-pc-based
35. *UK Climate: Historical Station Data* (UK Met Office, accessed 15 January 2015); http://www.metoffice.gov.uk/public/weather/climate-historic/#?tab=climateHistoric
36. Grenfell, B., Bjørnstad, O. & Kappey, J. Traveling waves and spatial hierarchies in measles epidemics. *Nature* **414,** 716–723 (2001).
37. Viboud, C. *et al.* Synchrony, waves, and spatial hierarchies in the spread of influenza. *Science* **312,** 447–451 (2006).
38. Keitt, T. & Fischer, J. Detection of scale-specific community dynamics using wavelets. *Ecology* **87,** 2895–2904 (2006).
39. Cazelles, B. *et al.* Wavelet analysis of ecological timeseries. *Oecologia* **156,** 287–304 (2008).
40. Bell, J. *et al.* Putting the brakes on a cycle: Bottom-up effects damp cycle amplitude. *Ecol. Lett.* **15,** 310–318 (2012).
41. Cazelles, B., Cazelles, K. & Chavez, M. Wavelet analysis in ecology and epidemiology: Impact of statistical tests. *J. R. Soc. Interface* **11,** 20130585 (2014).
42. Rouyer, T., Fromentin, J., Stenseth, N. & Cazelles, B. Analysing multiple time series and extending significance testing in wavelet analysis. *Mar. Ecol. Prog. Ser.* **359,** 11–23 (2008).
43. Torrence, C. & Compo, G. P. A practical guide to wavelet analysis. *Bull. Am. Meteorol. Soc.* **79,** 61–78 (1998).
44. Addison, P. S. *The Illustrated Wavelet Transform Handbook: Introductory Theory and Applications in Science, Engineering, Medicine and Finance* (Taylor and Francis, 2002).
45. Meyers, S., Kelly, B. & O'Brien, J. An introduction to wavelet analysis in oceanography and meteorology: With application to the dispersion of yanai waves. *Mon. Weath. Rev.* **121,** 2858–2866 (1993).
46. Bandrivskyy, A., Bernjak, A., McClintock, P. V. E. & Stefanovska, A. Wavelet phase coherence analysis: Application to skin temperature and blood flow. *Cardiovasc. Eng.* **4,** 89–93 (2004).
47. Stefanovska, A. Coupled oscillators—complex but not complicated cardiovascular and brain interactions. *IEEE Eng. Med. Biol.* **26,** 25–29 (2007).
48. Theiler, J., Eubank, S., Longtin, A., Galdrikian, B. & Farmer, J. Testing for nonlinearity in time series: The method of surrogate data. *Physica D* **58,** 77–94 (1992).
49. Prichard, D. & Theiler, J. Generating surrogate data for time series with several simultaneously measured variables. *Phys. Rev. Lett.* **73,** 951–954 (1994).
50. Jones, J., Doran, P. & Holmes, R. Climate and food synchronize regional forest bird abundances. *Ecology* **84,** 3024–3032 (2003).
51. Grøtan, V. *et al.* Climate causes large-scale spatial synchrony in population fluctuations of a temperate herbivore. *Ecology* **86,** 1472–1482 (2005).
52. Sæther, B. *et al.* The extended Moran effect and large-scale synchronous fluctuations in the size of great tit and blue tit populations. *J. Anim. Ecol.* **76,** 315–325 (2007).
53. Schreiber, T. & Schmitz, A. Surrogate time series. *Physica D* **142,** 346–382 (2000).
54. Sakia, R. The Box–Cox transformation technique: A review. *Statistician* **41,** 169–178 (1992).